

Self-Evolving Depth-Supervised 3D Gaussian Splatting from Rendered Stereo Pairs

Sadra Safadoust^{1*}

<https://sadrasafa.github.io/>

Fabio Tosi²

<https://fabiotosi92.github.io/>

Fatma Güney¹

<https://mysite.ku.edu.tr/fguney/>

Matteo Poggi²

<https://mattpoggi.github.io/>

¹ Department of Computer Engineering and KUIS AI Center, Koç University, Istanbul, Turkey

² Department of Computer Science and Engineering (DISI), University of Bologna, Italy

* project started while visiting University of Bologna

Abstract

3D Gaussian Splatting (GS) significantly struggles to accurately represent the underlying 3D scene geometry, resulting in inaccuracies and floating artifacts when rendering depth maps. In this paper, we address this limitation, undertaking a comprehensive analysis of the integration of depth priors throughout the optimization process of Gaussian primitives, and present a novel strategy for this purpose. This latter dynamically exploits depth cues from a readily available stereo network, processing virtual stereo pairs rendered by the GS model itself during training and achieving consistent self-improvement of the scene representation. Experimental results on three popular datasets, breaking ground as the first to assess depth accuracy for these models, validate our findings.

Project page: <https://kuis-ai.github.io/StereoGS/>



Figure 1: **Self-Evolving Depth-Supervised 3D Gaussian Splatting (GS) in action.** Our strategy allows GS to self-improve during optimization, and to render better depth maps.

1 Introduction

In recent years, NeRF [1] has deeply revolutionized several aspects of computer vision, introducing innovative paradigms and redefining our understanding of the field. First and

foremost, NeRF has represented a turning point for image rendering and novel view synthesis [37, 40, 48], casting these tasks as the optimization of a continuous 3D representation of the scene encoded in multi-layer perceptrons (MLPs), queried with (x, y, z) coordinates in space and (θ, ϕ) view angles to predict color and opacity for any generic 3D point. Rendering is achieved by casting rays and accumulating colors and opacities along them into pixels.

However, the recent advent of 3D Gaussian Splatting (GS) [24] is rapidly conquering the main stage at the expense of NeRF, due to the much lower time required for both optimization and rendering. While GS has certainly advanced the state-of-the-art in terms of photorealism and rendering speed, the underlying geometry modeled by the Gaussians does not reflect the same quality as the rendering. This is evident in the depth maps generated by GS itself – by replacing the color components of the Gaussians with their position during the rendering process – as we can notice in Fig. 1, where examples from BlendedMVS and ETH3D are affected by several floaters and artifacts. Some works from the literature [2, 13, 51, 53, 58] show evidence that using depth priors as a form of additional supervision when optimizing a NeRF can improve the quality of the rendered images, especially when very few images are available for training. Intuitively, this strategy also has the potential to improve the underlying geometry encoded by the NeRF itself, although no attention has been paid to this by prior works, nor to the different, possible approaches for retrieving depth priors from the very same images used to train NeRF – and to the intrinsic limitation each choice brings.

In this paper, we first delve into a study of Depth-Supervised 3D Gaussian Splatting (DS-GS) variants by examining and measuring the impact that different depth-from-image solutions have on the optimization of both the appearance and geometry modeled by GS. Specifically, we review four main strategies for extracting depth priors from the multiple images involved in GS optimization: i) Structure-from-Motion (SfM) [55], ii) Monocular Depth Estimation (MDE) [7], iii) Depth Completion (DC) [6], and iv) Multi-View Stereo (MVS) [56]. Each one has its peculiar strengths, as well as its weaknesses. To name a few: on the one hand, SfM and MVS suffer in the presence of sparse views where the overlap between images is small; on the other hand, single-image approaches are free from this constraint, yet assume a network that can generalize properly across very different scenarios.

In addition to this exploration, we propose a novel approach to improve GS optimization, still by exploiting the supervision of depth priors, this time obtained by a fifth strategy that is a cornerstone of computer vision, but not included in the previous list: *stereo matching*. Indeed, we argue that despite the inaccurate underlying geometry modeled by the Gaussians, GS can still render geometrically consistent images – e.g., rectified stereo images, even when a stereo camera is unavailable. Accordingly, GS can be employed to generate frames, which can then be processed by a pre-trained deep stereo network [54] to obtain the supplementary supervision required to enhance the underlying geometry of GS itself. Thanks to the efficient rasterization process of GS, we can carry this out directly during the optimization, deploying a new GS framework capable of *self-evolving*, supported by this external stereo network.

Experiments on ETH3D [56], ScanNet++ [23] and BlendedMVS [22] support our claims:

- We carry out a comparison between different strategies for retrieving depth priors from images, by evaluating the impact of each on improving both the appearance and geometry modeled by DS-GS against vanilla GS.
- We propose a new Self-Evolving GS framework, capable of supervising itself through depth priors retrieved by a stereo matching network, processing the rectified images rendered by the GS itself during training.
- Compared to the use of depth priors from classical strategies, our approach renders both better images and depth maps in real, sparse view settings.

2 Related Work

In this section, we present a review of the literature relevant to our study.

Novel View Synthesis. Generating realistic novel views from 3D scene representations has been an active area of research. Early approaches used geometries such as meshes [26, 49, 50], planes [24], and point clouds [69, 79] to model scenes. More recently, neural radiance fields (NeRFs) [40], extensively discussed in [11, 12, 45], have emerged as a highly effective representation for photorealistic novel view synthesis. NeRF models the scene as an implicit, continuous radiance field, allowing fine-grained detail to be captured. Several extensions to the original NeRF formulation have enhanced rendering quality by improving anti-aliasing [3, 4, 5], modeling reflectance more accurately [9, 21, 62], training with sparse views [61, 43, 68], and reducing computational overhead during training [12, 27, 42, 48, 59] and rendering time [18, 65, 75]. In parallel, point cloud-based representations [69, 74, 79] have gained popularity due to their rendering efficiency. In addition, recent differentiable point splatting techniques, such as 3D GS [29], have enabled state-of-the-art real-time scene rendering. Among others, NeRF was used to generate stereo images for training stereo networks [60]. Our work has a different goal – to generate stereo pairs and supervise GS itself.

Image-based Depth Estimation. Traditionally, depth estimation from images has relied on non-learning-based approaches. Among them, Structure-from-Motion [11, 20, 64] estimates both the sparse 3D structure of a scene and the camera poses from a set of images, with COLMAP [64] becoming a reference pipeline for the community in the last decade. When poses are known already, Multi-View Stereo [15, 67] used feature matching and geometric constraints – i.e., epipolar geometry – across multiple views, while binocular stereo [23, 62] relied on correspondences between rectified stereo pairs. However, the field has undergone a revolutionary transformation with the advent of deep learning. In the context of multi-view [68, 65, 70] and binocular stereo [22, 44, 61, 81], learning-based approaches have leveraged the capabilities of convolutional neural networks to extract robust feature representations for more accurate correspondence estimation. This infusion of deep learning has not only increased accuracy, but has also facilitated the refinement and completion of sparse/noisy depth maps [25, 25, 30, 67], effectively filling in holes or refining inaccuracies. Within this paradigm, monocular depth estimation [8, 68, 41, 80] has emerged as a specialized subset, where deep neural networks are trained to directly predict depth out of a single image, typically on large datasets where pseudo-ground truth depth is available [46, 47].

Radiance Fields with Depth Priors. While successful in image rendering, challenges arise in representing accurate scene geometries using advances in radiance fields. In response, supervised approaches incorporating depth priors have recently emerged. As a precursor, DS-NeRF [12] employs depth supervision using sparse point clouds from COLMAP during training. In parallel, Rossle et al. [61] employ dense depth priors by densifying sparse depth data extracted from COLMAP. In NerfingMVS [66], instead, COLMAP extracts sparse depth priors, subsequently utilized to fine-tune a pretrained monocular depth network that is then employed to supervise volume sampling. PointNeRF [69] introduces an intermediate step using feature point clouds and demonstrates improved efficiency compared to the vanilla NeRF. To the same end, CorresNeRF [52] uses adaptive correspondence generation, while MonoSDF [76] improves the reconstruction process by incorporating depth and normal cues predicted by general-purpose monocular estimators. Similarly, SparseNeRF [64] leverages depth priors from real-world inaccurate observations, which can be from pre-trained depth models or coarse depth maps of consumer-level depth sensors, while some approaches used depth priors when dealing with dynamic scenes [46, 49]. In a concurrent effort, Chung et al.

[□] represents the only attempt to regularize GS using monocular depth networks. However, our paper highlights that better priors can be exploited to this end.

3 Background Theory

3.1 3D Gaussian Splatting (GS)

3D Gaussian Splatting is a groundbreaking technique in the domain of explicit radiance fields and computer graphics. This unique approach relies on the incorporation of millions of 3D Gaussians, which marks a shift from the prevailing methods used in neural radiance field.

Learning starts with multi-view images, by estimating camera poses and (optionally) sparse 3D points to bootstrap GS, which optimizes a set $\mathcal{G} = \{g_1, g_2, \dots, g_{\mathcal{N}}\}$ of 3D Gaussians, where \mathcal{N} is the number of Gaussians in the scene. Each Gaussian, denoted as g_i , is characterized by a full 3D covariance matrix $\Sigma_i \in \mathbb{R}^{3 \times 3}$, center position $\boldsymbol{\mu}_i \in \mathbb{R}^3$, opacity $o_i \in [0, 1]$, and color \mathbf{c}_i , which is represented by spherical harmonics (SH) for a view-dependent appearance. Backpropagation can be used to learn and optimize all these properties. The spatial influence of a single Gaussian primitive can be expressed as follows:

$$g_i(\mathbf{x}) = e^{-\frac{1}{2}(\mathbf{x}-\boldsymbol{\mu}_i)^\top \Sigma_i^{-1}(\mathbf{x}-\boldsymbol{\mu}_i)} \quad (1)$$

Here, the spatial covariance Σ defines an ellipsoid as $\Sigma = \mathbf{R}\mathbf{S}\mathbf{S}^\top \mathbf{R}^\top$, where $\mathbf{S} \in \mathbb{R}^3$ represents the spatial scale and $\mathbf{R} \in \mathbb{R}^{3 \times 3}$ represents the rotation, parameterized by a quaternion.

For rendering, GS operates similarly to NeRF but deviates significantly in the computation of blending coefficients. This involves the "splatting" of 3D Gaussian points onto a 2D image plane, as $\Sigma' = \mathbf{J}\mathbf{W}\Sigma\mathbf{W}^\top \mathbf{J}^\top$ and $\boldsymbol{\mu}' = \mathbf{J}\mathbf{W}\boldsymbol{\mu}$. Then, pixel color C is obtained by merging 3D Gaussian splats that overlap, sorted by depth:

$$C = \sum_{i \in \mathcal{N}} \mathbf{c}_i \alpha_i \prod_{j=1}^{i-1} (1 - \alpha_j) \quad \text{with} \quad \alpha_i = o_i \exp\left(-\frac{1}{2}(\mathbf{x}' - \boldsymbol{\mu}'_i)^\top \Sigma_i'^{-1}(\mathbf{x}' - \boldsymbol{\mu}'_i)\right) \quad (2)$$

The optimization process begins either from Structure-from-Motion (SfM) point clouds or random 3D points. Then, Stochastic Gradient Descent (SGD) is employed, with L1 and D-SSIM loss functions between real and rendered views. Analogously to color, the resulting depth D can be determined by replacing \mathbf{c}_i with d_i – i.e., the distance of g_i from the camera.

3.2 Depth from Images

In this section, we review established methodologies for estimating depth from images tailored for GS setting – i.e., multiple images captured from different viewpoints using a single camera – allowing to implement Depth-Supervised 3D Gaussian Splatting (DS-GS) variants.

Structure-from-Motion (SfM). It aims at reconstructing 3D structure and camera positions from a set of images, starting with two-view triangulation:

$$\mathbf{X}_{ij} \sim \tau(\tilde{\mathbf{x}}_i, \tilde{\mathbf{x}}_j, \mathbf{P}_i, \mathbf{P}_j) \quad \text{with} \quad i \neq j \quad (3)$$

with \mathbf{X}_{ij} being a generic 3D point visible from images $\mathbf{I}_i, \mathbf{I}_j$, $\tilde{\mathbf{x}}_i, \tilde{\mathbf{x}}_j$ its pixel coordinates on the two images, $\mathbf{P}_i, \mathbf{P}_j$ their camera poses, and τ a generic triangulation method. Usually, $\tilde{\mathbf{x}}_i, \tilde{\mathbf{x}}_j$ pairs are identified in advance by extracting features and matching them. Eventually, global optimization is carried out with bundle adjustment, minimizing the reprojection error E

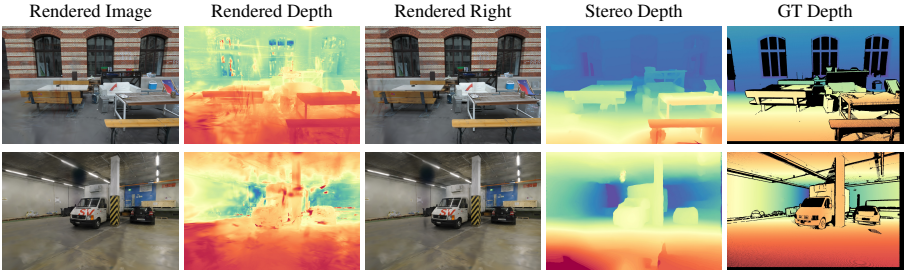


Figure 2: **Depth priors retrieved from stereo.** Vanilla GS produces noisy and inaccurate depths, yet can render stereo pairs for getting strong depth priors as additional supervision.

$$E = \sum_j \|\pi(\mathbf{P}_i, \mathbf{X}_i) - \mathbf{x}_j\|_2^2 \quad (4)$$

with π being the projection function from 3D to image space. SfM algorithms – COLMAP [54] in particular – are the foundation for bootstrapping GS optimization, providing both the camera poses and the 3D points for initializing the Gaussians.

Depth Completion (DC). This method aims to recover a dense depth map from a set of sparse measurements \mathbf{X}_i , usually guided by a color image \mathbf{I}_i , with a network Θ_{DC} :

$$\mathbf{D}_{\text{DC}}(\mathbf{I}_i) = \Theta_{\text{DC}}(\mathbf{I}_i, \mathbf{X}_i) \quad (5)$$

In our setting, a DC model can process the sparse set of points estimated by COLMAP and projected over the images, similarly to [54] in principle. From a practical perspective, the availability of a DC model capable of generalizing across scenes and levels of sparsity is crucial for this purpose – although ignored in [54].

Multi-View Stereo (MVS). A dense depth map can be obtained by matching pixels across multiple, posed images along epipolar lines. This task is nowadays tackled with deep networks as well [41], with a generic model Θ_{MVS} processing a reference image \mathbf{I}_i and a set of N source views, given their poses

$$\mathbf{D}_{\text{MVS}}(\mathbf{I}_i) = \Theta_{\text{MVS}}(\mathbf{I}_i, \mathbf{P}_i, \{\mathbf{I}_j, \mathbf{P}_j\}_j^N) \quad (6)$$

Despite the outstanding accuracy reached in the last years, MVS networks still struggle when dealing with sparse views with limited overlap, and may suffer from generalization issues.

Monocular Depth Estimation (MDE). With the rise of deep learning, estimating the depth of a single image has become a reality. Nowadays, state-of-the-art models are trained over millions of images to predict *affine-invariant* depth [46, 42]:

$$\mathbf{D}_{\text{MDE}}(\mathbf{I}_i) = m \cdot \Theta_{\text{MDE}}(\mathbf{I}_i) + q \quad (7)$$

where m and q are respectively *scale* and *shift* factors required to recover the effective scale within the relative depth map predicted by the model Θ_{MDE} . In our specific setting, m and q can be directly derived by fitting the predicted depth map on the COLMAP depth points through least squares. A concurrent work [10] also follows this strategy to regularize GS optimization – yet without measuring its impact on the underlying geometry.

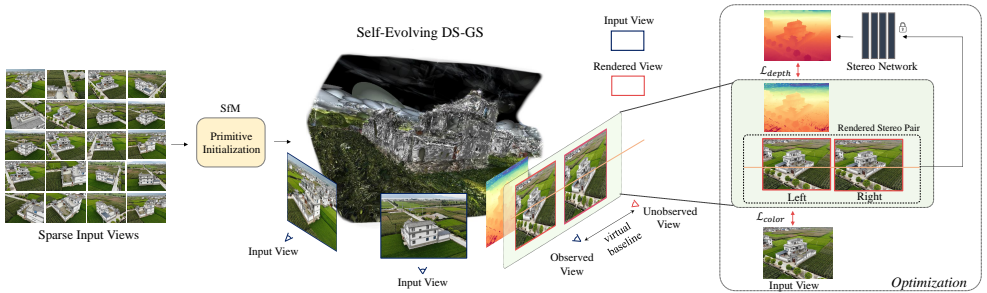


Figure 3: **Self-Evolving DS-GS pipeline.** As soon as GS can render stable images, we render *stereo pairs*, estimate depth with a pre-trained network, and use it to compute \mathcal{L}_{depth} .

4 Self-Evolving Depth-Supervised GS from Stereo

In this section, we introduce an alternative strategy to obtain dense depth priors and improve the optimization process of GS. We begin with the empirical observation that, despite its inaccurate underlying geometry, GS can render images that exhibit *geometric consistency*.

This means that a trained GS can render frames over which we can run conventional depth-from-images algorithms to retrieve quite accurate depth priors for supervising the GS itself. Purposely, the simplest strategy consists of rendering *rectified stereo pairs* – i.e., images captured from two viewpoints shifted by a horizontal offset – and then estimating depth through triangulation from disparity. Fig. 2 shows qualitative evidence of the effectiveness of this strategy: while vanilla GS renders noisy depth maps, a pre-trained stereo model can generate much better depth maps from stereo pairs rendered by vanilla GS itself.

For this purpose, given any camera pose \mathbf{P}_i , we can derive a corresponding right viewpoint with pose \mathbf{R}_i in a fictitious stereo configuration, according to an arbitrary baseline b :

$$\mathbf{R}_i = \begin{pmatrix} \mathbb{I} & \mathbf{t} \\ 0 & 1 \end{pmatrix} \cdot \mathbf{P}_i \quad \text{with} \quad \mathbf{t} = (b \ 0 \ 0)^\top \quad (8)$$

Then, for each image \mathbf{I}_i in the training set, we can render a corresponding right frame \mathbf{I}'_i , estimate disparity with a stereo network Θ and use the focal length f to triangulate depth:

$$\mathbf{D}_{\text{stereo}}(\mathbf{I}_i) = \frac{f \cdot b}{\Theta(\mathbf{I}_i, \mathbf{I}'_i)} \quad (9)$$

Fig. 3 provides an overview of our approach. During GS training, we can start exploiting this strategy only after the model can render good-quality images already – i.e., after T steps. Furthermore, as disparity estimation requires a non-negligible extra computation, we cache disparity maps as soon as they are computed the first time and reuse them in the subsequent steps; as long as the quality of rendered images increases with training, we set a refresh interval τ for rendering again the stereo pairs and updating the disparity priors.

Why stereo? Our strategy would work to render views for MVS networks as well, however: i) as we aim at minimizing the overhead during GS optimization, frame pairs are the minimum amount of information required to derive depth from images through geometry; ii) tuning a single parameter for rendering the novel, arbitrary views – i.e., the horizontal baseline b – is simpler than tuning 6-DoF poses; iii) state-of-the-art stereo networks excel at domain generalization, whereas we observed this is often not true for MVS networks.

5 Experiments

In this section, we present the approaches we selected to obtain depth priors and the datasets used in our experiments. Next, we describe the implementation details of our framework. Finally, we report our findings.

5.1 Depth Priors Settings

To evaluate the effectiveness of the different strategies for extracting depth priors from images, we select one representative method for each. **SfM**: We use COLMAP [54], as it is already used for computing camera poses and the initial 3D points from which GS optimization is bootstrapped. **DC**: We select VPPDC [9] since, to the best of our knowledge, it is the only depth completion approach proposed for cross-domain generalization. **MDE**: We use ZoeDepth [7], with the weights provided by the authors. The same model has been used in a concurrent work [11], allowing us to assess its effectiveness against alternative depth priors sources. **MVS**: We use CER-MVS [56], as it shows promising generalization. We use BlendedMVS weights for tests on ETH3D/ScanNet++, and DTU weights on BlendedMVS, to avoid overlap with training data. **Stereo (Self-Evolving)**: We use the RAFT-Stereo [52] variant trained for the Robust Vision Challenge – iRAFT-Stereo_RVC [28].

5.2 Datasets

We select three datasets providing ground-truth depth, instrumental for our studies. We will appreciate how the differences in the three will impact the results by different methods.

ETH3D. It is a real-world dataset, providing images and ground truth depth at about 24 Megapixels. We use all of the 13 training scenes of the high-resolution set, having 14 to 76 images. We use the provided undistorted images, camera poses, and point clouds. Following vanilla GS settings, images are resized to have 1600 width before training. We manually split each scene into training and test sets (please check the **supplementary** for details of the splits). We align (distorted) ground truth depth to undistorted images for evaluation.

ScanNet++. It is a real-world dataset with high-fidelity 3D geometry and high-resolution RGB images of indoor scenes. We perform our experiments on 2 of the randomly selected scenes, due to the large number of sequences. We undistort the fisheye images and depth maps using the provided official toolkit. The scenes contain 291 and 399 images at a resolution of 1752×1168 , and we only use every 10th image for training and the rest for testing.

BlendedMVS. It is a semi-synthetic dataset. Due to the large number of sequences, we randomly select 4 of them and perform experiments on these sequences. Since this dataset does not provide the point clouds, we run COLMAP on the images using the given camera poses to obtain the point clouds for bootstrapping GS. We use the images at their original resolution of 768×576 , counting 75 to 212 frames per scene, with every 4th used for testing.

5.3 Implementation Details

We implement our self-evolving GS starting from [29]. The loss for DS-GS is defined as:

$$\mathcal{L} = (1 - \lambda_1) \|\mathbf{I} - \hat{\mathbf{I}}\|_1 + \lambda_1 \text{D-SSIM}(\mathbf{I}, \hat{\mathbf{I}}) + \lambda_2 \|\mathbf{D}_k(\mathbf{I}) - \hat{\mathbf{D}}\|_1 \quad (10)$$

where \mathbf{I} is the original image, $\hat{\mathbf{I}}$ and $\hat{\mathbf{D}}$ are the rendered image and depth maps, respectively, and \mathbf{D}_k is the depth map, obtained through one of the proposed methods. e.g., for our self-

Method	Depth			View Synthesis			
	Abs. Rel. ↓	RMSE ↓	$\delta < 1.25 \uparrow$	SSIM ↑	PSNR ↑	LPIPS ↓	
GS [14]	0.211	1.698	0.652	0.7425	20.4029	0.3385	
DS-GS	+ SfM [12]	0.109	0.870	0.844	0.7561	21.7224	0.3261
	+ DC [1]	0.148	1.272	0.828	0.7557	21.5206	0.3248
	+ MDE [1]	0.153	1.204	0.793	0.7475	21.3104	0.3377
	+ MVS [15]	0.094	1.031	0.914	0.7692	22.2806	0.3105
	+ Self-Evolving (ours)	0.057	0.599	0.942	0.7704	22.2825	0.3141
+ Oracle (GT depth)	0.020	0.317	0.980	0.7764	22.4669	0.3009	

Table 1: Quantitative Results on ETH3D.

Method	Depth			View Synthesis			
	Abs. Rel. ↓	RMSE ↓	$\delta < 1.25 \uparrow$	SSIM ↑	PSNR ↑	LPIPS ↓	
GS [14]	0.154	0.416	0.735	0.9162	27.7907	0.1587	
DS-GS	+ SfM [12]	0.104	0.295	0.860	0.9131	27.9140	0.1663
	+ DC [1]	0.144	0.381	0.813	0.9145	27.5081	0.1659
	+ MDE [1]	0.083	0.242	0.926	0.9168	28.0568	0.1588
	+ MVS [15]	0.152	0.437	0.824	0.9138	27.3536	0.1699
	+ Self-Evolving (ours)	0.068	0.222	0.928	0.9165	28.1488	0.1601
+ Oracle (GT depth)	0.024	0.103	0.983	0.9199	28.6413	0.1539	

Table 2: Quantitative Results on ScanNet++.

evolving method $\mathbf{D}_k = \mathbf{D}_{\text{Stereo}}$. We set $\lambda_1 = 0.2$ and set $\lambda_2 = 0.01$ for the BlendedMVS dataset and $\lambda_2 = 0.1$ for the ETH3D and ScanNet++ datasets. Note that for our self-evolving method, we set $\lambda_2 = 0$ for all iterations before the starting step T . On the BlendedMVS dataset, we use $T = 17K$ and train the models for 20K iterations, while for the ETH3D and ScanNet++ datasets, we set $T = 7K$ and train for 11K iterations. In all datasets, we set the refresh interval to $\tau = 100$ and randomly sample b from an interval (see **supplementary material**). We perform all of our experiments on a single V100 GPU.

5.4 Results

In this section, we report the outcome of our experiments. In each table, we highlight the **first**, **second** and **third** -best results.

ETH3D. Table 1 shows quantitative results on ETH3D. We can appreciate how any DS-GS variant improves over vanilla GS, both in terms of depth and color rendering quality. Using COLMAP yields the third-best result and unveils an interesting finding: vanilla GS optimization is sub-optimal since the very same 3D points used to bootstrap Gaussians can provide additional supervision for free. Nonetheless, DC fails at improving over COLMAP, because of the very few SfM points being insufficient for obtaining a good-quality dense depth map – see the **supplementary material** for qualitative examples. MVS ranks second both in terms of depth and color quality, while our self-evolving DS-GS largely outperforms it in terms of depth estimation, slightly improving color quality in SSIM and PSNR as well.

ScanNet++. Table 2 collects results on ScanNet++. At first glance, we can confirm the superiority of our approach in terms of depth metrics, while resulting almost equivalent to MDE on color metrics. Interestingly, MDE significantly outperforms SfM and other methods in this setting. This is caused by the lack of texture in these scenes, on which COLMAP extracts few 3D points (see **supplementary material**) and thus provides poor supervision.

Method	Depth			View Synthesis			
	Abs. Rel. ↓	RMSE ↓	$\delta < 1.25 \uparrow$	SSIM ↑	PSNR ↑	LPIPS ↓	
GS [24]	0.058	7.041	0.933	0.6301	21.6160	0.2729	
DS-GS	+ SfM [27]	0.021	3.910	0.990	0.6389	22.1409	0.2644
	+ DC [9]	0.021	3.719	0.991	0.6378	21.9899	0.2648
	+ MDE [9]	0.113	12.141	0.840	0.6142	21.1857	0.2867
	+ MVS [36]	0.065	10.316	0.914	0.6021	20.8971	0.2944
	+ Self-Evolving (ours)	0.020	3.714	0.992	0.6377	21.9734	0.2696
+ Oracle (GT depth)	0.013	2.645	0.993	0.6480	22.2282	0.2575	

Table 3: Quantitative Results on BlendedMVS.



Figure 4: Qualitative Results on ETH3D.

BlendedMVS. Table 3 collects results on BlendedMVS. On these semi-synthetic images, SfM can extract very dense matches, resulting in much stronger supervision as well as a much simpler completion task for the DC model (see **supplementary material**). Indeed, DC ranks second in both depth and color metrics, with SfM ranking first in rendering quality. On the contrary, our solution is, again, the absolute winner in terms of depth accuracy, while MDE and MVS fail at improving the baseline: we ascribe this to generalization issues.

Qualitative Results. We conclude this section by reporting some qualitative comparisons. Fig. 4 collects three samples from ETH3D dataset. At the very top, we show images and depth maps obtained by the vanilla GS, with several artifacts appearing in any of the three examples, followed by results yielded by using SfM or our strategy. Conversely to SfM, our self-evolving GS can consistently improve both rendered images and depth maps. Finally, at the very bottom, we report ground-truth images and depth maps as a reference. We report more qualitative results in the **supplementary material**.

5.5 Ablation Studies

Finally, we conduct some ablation studies focused on our self-evolving framework. These are carried out on the BlendedMVS dataset and averaged over 5 runs.

Stereo Models. Table 4 collects the results achieved by using different stereo networks to obtain depth priors. For each model, we report the specific weights we used among those available in brackets. We can appreciate how using any of the state-of-the-art stereo back-

Method	Depth			View Synthesis			
	Abs. Rel. ↓	RMSE ↓	$\delta < 1.25 \uparrow$	SSIM ↑	PSNR ↑	LPIPS ↓	
GS [43]	0.058	7.041	0.933	0.6301	21.6160	0.2729	
+ Self-Ev.	IGEV-Stereo [45] (Middlebury [46])	0.025	4.331	0.984	0.6340	21.8255	0.2727
	PCVNet [47] (SceneFlow [48])	0.023	4.082	0.988	0.6351	21.8605	0.2717
	CREStereo [45] (Mixed)	0.023	3.896	0.985	0.6361	21.9168	0.2714
	iRaftStereo_RVC [49] (Mixed)	0.020	3.714	0.992	0.6377	21.9734	0.2696

Table 4: Ablation Studies on BlendedMVS – stereo models.

Method	Depth			View Synthesis			
	Abs. Rel. ↓	RMSE ↓	$\delta < 1.25 \uparrow$	SSIM ↑	PSNR ↑	LPIPS ↓	
GS [43]	0.058	7.041	0.933	0.6301	21.6160	0.2729	
+ Self-Ev.	RAFT-Stereo [50] (NerfStereo [51])	0.023	4.046	0.987	0.6360	21.8964	0.2715
	RAFT-Stereo [50] (SceneFlow [48])	0.020	3.679	0.991	0.6375	21.9517	0.2696
	RAFT-Stereo [50] (Middlebury [46])	0.021	3.929	0.989	0.6362	21.9027	0.2708
	iRaftStereo_RVC [49] (Mixed)	0.020	3.714	0.992	0.6377	21.9734	0.2696

Table 5: Ablation Studies on BlendedMVS – RAFT-Stereo variants.

bones allows for largely improving the results over vanilla GS. However, iRAFTStereo_RVC and CREStereo show higher improvements against PCVNet and IGEV-Stereo, both in terms of color and depth rendering. We ascribe this both to their specific architecture, as well as to the mix of several datasets used to train them.

RAFT-Stereo – Training Datasets. To figure out the real impact of both the training data and the stereo backbone, in Table 5 we compare the results obtained with different RAFT-Stereo weights. The gap between the several instances is very low, with iRAFT-Stereo and the original RAFT-Stereo trained on SceneFlow being on par on three out of six metrics.

6 Conclusion

In summary, this work seeks to address a critical limitation in 3D Gaussian Splatting by focusing on improving its underlying scene geometry. Through a comprehensive analysis, we study an optimization approach that integrates external depth priors, simultaneously improving the inferred 3D structure and the quality of novel view synthesis. A key contribution is our novel strategy leveraging depth priors computed from readily available deep stereo networks on virtual stereo pairs rendered during training by GS itself, demonstrating superior performance compared to alternative depth-from-image solutions. Experimental results on ETH3D, ScanNet++, and BlendedMVS datasets support the importance of our findings and provide evidence for the effectiveness of our proposal.

Acknowledgements. We acknowledge the CINECA award under the ISCRA initiative, for the availability of high-performance computing resources and support. Sadra Safadoust was supported by KUIS AI Fellowship and UNVEST R&D Center. This project is co-funded by the European Union (ERC, ENSURE, 101116486). Views and opinions expressed are however those of the author(s) only and do not necessarily reflect those of the European Union or the European Research Council. Neither the European Union nor the granting authority can be held responsible for them.

References

- [1] Sameer Agarwal, Noah Snavely, Ian Simon, Steven M. Seitz, and Richard Szeliski. Building rome in a day. In *2009 IEEE 12th International Conference on Computer Vision*, pages 72–79, 2009.
- [2] Benjamin Attal, Eliot Laidlaw, Aaron Gokaslan, Changil Kim, Christian Richardt, James Tompkin, and Matthew O’Toole. Törf: Time-of-flight radiance fields for dynamic scene view synthesis. *Advances in Neural Information Processing Systems*, 34, 2021.
- [3] Jonathan T Barron, Ben Mildenhall, Matthew Tancik, Peter Hedman, Ricardo Martin-Brualla, and Pratul P Srinivasan. Mip-nerf: A multiscale representation for anti-aliasing neural radiance fields. In *Proceedings of the IEEE/CVF International Conference on Computer Vision*, pages 5855–5864, 2021.
- [4] Jonathan T Barron, Ben Mildenhall, Dor Verbin, Pratul P Srinivasan, and Peter Hedman. Mip-nerf 360: Unbounded anti-aliased neural radiance fields. In *Proceedings of the IEEE/CVF Conference on Computer Vision and Pattern Recognition*, pages 5470–5479, 2022.
- [5] Jonathan T Barron, Ben Mildenhall, Dor Verbin, Pratul P Srinivasan, and Peter Hedman. Zip-nerf: Anti-aliased grid-based neural radiance fields. *arXiv preprint arXiv:2304.06706*, 2023.
- [6] Luca Bartolomei, Matteo Poggi, Andrea Conti, Fabio Tosi, and Stefano Mattoccia. Revisiting depth completion from a stereo matching perspective for cross-domain generalization. In *International Conference on 3D Vision (3DV)*, March 2024.
- [7] Shariq Farooq Bhat, Reiner Birkel, Diana Wofk, Peter Wonka, and Matthias Müller. Zoedepth: Zero-shot transfer by combining relative and metric depth. *arXiv preprint arXiv:2302.12288*, 2023.
- [8] Amlaan Bhoi. Monocular depth estimation: A survey. *arXiv preprint arXiv:1901.09402*, 2019.
- [9] Xiaoxue Chen, Junchen Liu, Hao Zhao, Guyue Zhou, and Ya-Qin Zhang. Nerf: 3d reconstruction and view synthesis for transparent and specular objects with neural refractive-reflective fields. *arXiv preprint arXiv:2309.13039*, 2023.
- [10] Jaeyoung Chung, Jeongtaek Oh, and Kyoung Mu Lee. Depth-regularized optimization for 3d gaussian splatting in few-shot images. *arXiv preprint arXiv:2311.13398*, 2023.
- [11] Frank Dellaert and Lin Yen-Chen. Neural volume rendering: Nerf and beyond. *arXiv preprint arXiv:2101.05204*, 2020.
- [12] Kangle Deng, Andrew Liu, Jun-Yan Zhu, and Deva Ramanan. Depth-supervised nerf: Fewer views and faster training for free. In *Proceedings of the IEEE/CVF Conference on Computer Vision and Pattern Recognition*, pages 12882–12891, 2022.
- [13] Kangle Deng, Andrew Liu, Jun-Yan Zhu, and Deva Ramanan. Depth-supervised NeRF: Fewer views and faster training for free. In *Proceedings of the IEEE/CVF Conference on Computer Vision and Pattern Recognition (CVPR)*, June 2022.

- [14] Sara Fridovich-Keil, Alex Yu, Matthew Tancik, Qinhong Chen, Benjamin Recht, and Angjoo Kanazawa. Plenoxels: Radiance fields without neural networks. In *Proceedings of the IEEE/CVF Conference on Computer Vision and Pattern Recognition*, pages 5501–5510, 2022.
- [15] Yasutaka Furukawa, Carlos Hernández, et al. Multi-view stereo: A tutorial. *Foundations and Trends® in Computer Graphics and Vision*, 9(1-2):1–148, 2015.
- [16] Chen Gao, Ayush Saraf, Johannes Kopf, and Jia-Bin Huang. Dynamic view synthesis from dynamic monocular video. In *Proceedings of the IEEE/CVF International Conference on Computer Vision*, pages 5712–5721, 2021.
- [17] Kyle Gao, Yina Gao, Hongjie He, Denning Lu, Linlin Xu, and Jonathan Li. Nerf: Neural radiance field in 3d vision, a comprehensive review. *arXiv preprint arXiv:2210.00379*, 2022.
- [18] Stephan J Garbin, Marek Kowalski, Matthew Johnson, Jamie Shotton, and Julien Valentin. Fastnerf: High-fidelity neural rendering at 200fps. In *Proceedings of the IEEE/CVF International Conference on Computer Vision*, pages 14346–14355, 2021.
- [19] Beerend GA Gerats, Jelmer M Wolterink, and Ivo AMJ Broeders. Dynamic depth-supervised nerf for multi-view rgb-d operating room videos. In *International Workshop on Predictive Intelligence In MEDicine*, pages 218–230. Springer, 2023.
- [20] Riccardo Gherardi, Michela Farenzena, and Andrea Fusiello. Improving the efficiency of hierarchical structure-and-motion. In *2010 IEEE Computer Society Conference on Computer Vision and Pattern Recognition*, pages 1594–1600, 2010.
- [21] Yuan-Chen Guo, Di Kang, Linchao Bao, Yu He, and Song-Hai Zhang. Nerfren: Neural radiance fields with reflections. In *Proceedings of the IEEE/CVF Conference on Computer Vision and Pattern Recognition*, pages 18409–18418, 2022.
- [22] Mohd Saad Hamid, NurulFajar Abd Manap, Rostam Affendi Hamzah, and Ahmad Fauzan Kadmin. Stereo matching algorithm based on deep learning: A survey. *Journal of King Saud University-Computer and Information Sciences*, 34(5):1663–1673, 2022.
- [23] Rostam Affendi Hamzah, Haidi Ibrahim, et al. Literature survey on stereo vision disparity map algorithms. *Journal of Sensors*, 2016, 2016.
- [24] Derek Hoiem, Alexei A Efros, and Martial Hebert. Automatic photo pop-up. In *ACM SIGGRAPH 2005 Papers*, pages 577–584. 2005.
- [25] Junjie Hu, Chenyu Bao, Mete Ozay, Chenyou Fan, Qing Gao, Honghai Liu, and Tin Lun Lam. Deep depth completion: a survey. *arXiv preprint arXiv:2205.05335*, 2022.
- [26] Ronghang Hu, Nikhila Ravi, Alexander C Berg, and Deepak Pathak. Worldsheet: Wrapping the world in a 3d sheet for view synthesis from a single image. In *Proceedings of the IEEE/CVF International Conference on Computer Vision*, pages 12528–12537, 2021.

- [27] Tao Hu, Shu Liu, Yilun Chen, Tiancheng Shen, and Jiaya Jia. Efficientnerf efficient neural radiance fields. In *Proceedings of the IEEE/CVF Conference on Computer Vision and Pattern Recognition*, pages 12902–12911, 2022.
- [28] Hualie Jiang, Rui Xu, and Wenjie Jiang. An improved raftstereo trained with a mixed dataset for the robust vision challenge 2022. *arXiv preprint arXiv:2210.12785*, 2022.
- [29] Bernhard Kerbl, Georgios Kopanas, Thomas Leimkühler, and George Drettakis. 3d gaussian splatting for real-time radiance field rendering. *ACM Transactions on Graphics*, 42(4), 2023.
- [30] Muhammad Ahmed Ullah Khan, Danish Nazir, Alain Pagani, Hamam Mokayed, Marcus Liwicki, Didier Stricker, and Muhammad Zeshan Afzal. A comprehensive survey of depth completion approaches. *Sensors*, 22(18):6969, 2022.
- [31] Mijeong Kim, Seonguk Seo, and Bohyung Han. Infonerf: Ray entropy minimization for few-shot neural volume rendering. In *Proceedings of the IEEE/CVF Conference on Computer Vision and Pattern Recognition*, pages 12912–12921, 2022.
- [32] Yixing Lao, Xiaogang Xu, Xihui Liu, Hengshuang Zhao, et al. Corresnerf: Image correspondence priors for neural radiance fields. *Advances in Neural Information Processing Systems*, 36, 2024.
- [33] Jiankun Li, Peisen Wang, Pengfei Xiong, Tao Cai, Ziwei Yan, Lei Yang, Jiangyu Liu, Haoqiang Fan, and Shuaicheng Liu. Practical stereo matching via cascaded recurrent network with adaptive correlation. In *Proceedings of the IEEE/CVF Conference on Computer Vision and Pattern Recognition*, pages 16263–16272, 2022.
- [34] Lahav Lipson, Zachary Teed, and Jia Deng. Raft-stereo: Multilevel recurrent field transforms for stereo matching. In *International Conference on 3D Vision (3DV)*, 2021.
- [35] Lingjie Liu, Jiatao Gu, Kyaw Zaw Lin, Tat-Seng Chua, and Christian Theobalt. Neural sparse voxel fields. *Advances in Neural Information Processing Systems*, 33:15651–15663, 2020.
- [36] Zeyu Ma, Zachary Teed, and Jia Deng. Multiview stereo with cascaded epipolar raft. In *Proceedings of the European conference on computer vision (ECCV)*, 2022.
- [37] Ricardo Martin-Brualla, Noha Radwan, Mehdi SM Sajjadi, Jonathan T Barron, Alexey Dosovitskiy, and Daniel Duckworth. Nerf in the wild: Neural radiance fields for unconstrained photo collections. In *Proceedings of the IEEE/CVF Conference on Computer Vision and Pattern Recognition*, pages 7210–7219, 2021.
- [38] Armin Masoumian, Hatem A Rashwan, Julián Cristiano, M Salman Asif, and Domènec Puig. Monocular depth estimation using deep learning: A review. *Sensors*, 22(14): 5353, 2022.
- [39] Nikolaus Mayer, Eddy Ilg, Philip Hausser, Philipp Fischer, Daniel Cremers, Alexey Dosovitskiy, and Thomas Brox. A large dataset to train convolutional networks for disparity, optical flow, and scene flow estimation. In *The IEEE Conference on Computer Vision and Pattern Recognition (CVPR)*, June 2016.

- [40] Ben Mildenhall, Pratul P. Srinivasan, Matthew Tancik, Jonathan T. Barron, Ravi Ramamoorthi, and Ren Ng. Nerf: Representing scenes as neural radiance fields for view synthesis. In *ECCV*, 2020.
- [41] Yue Ming, Xuyang Meng, Chunxiao Fan, and Hui Yu. Deep learning for monocular depth estimation: A review. *Neurocomputing*, 438:14–33, 2021.
- [42] Thomas Müller, Alex Evans, Christoph Schied, and Alexander Keller. Instant neural graphics primitives with a multiresolution hash encoding. *ACM Trans. Graph.*, 41(4):102:1–102:15, July 2022. doi: 10.1145/3528223.3530127. URL <https://doi.org/10.1145/3528223.3530127>.
- [43] Michael Niemeyer, Jonathan T Barron, Ben Mildenhall, Mehdi SM Sajjadi, Andreas Geiger, and Noha Radwan. Regnerf: Regularizing neural radiance fields for view synthesis from sparse inputs. In *Proceedings of the IEEE/CVF Conference on Computer Vision and Pattern Recognition*, pages 5480–5490, 2022.
- [44] Matteo Poggi, Fabio Tosi, Konstantinos Batsos, Philippos Mordohai, and Stefano Mattoccia. On the synergies between machine learning and binocular stereo for depth estimation from images: a survey. *IEEE Transactions on Pattern Analysis and Machine Intelligence*, 44(9):5314–5334, 2021.
- [45] AKM Rabby and Chengcui Zhang. Beyondpixels: A comprehensive review of the evolution of neural radiance fields. *arXiv preprint arXiv:2306.03000*, 2023.
- [46] René Ranftl, Alexey Bochkovskiy, and Vladlen Koltun. Vision transformers for dense prediction. *ICCV*, 2021.
- [47] René Ranftl, Katrin Lasinger, David Hafner, Konrad Schindler, and Vladlen Koltun. Towards robust monocular depth estimation: Mixing datasets for zero-shot cross-dataset transfer. *IEEE Transactions on Pattern Analysis and Machine Intelligence*, 44(3), 2022.
- [48] Christian Reiser, Songyou Peng, Yiyi Liao, and Andreas Geiger. Kilonerf: Speeding up neural radiance fields with thousands of tiny mlps. In *Proceedings of the IEEE/CVF International Conference on Computer Vision*, pages 14335–14345, 2021.
- [49] Gernot Riegler and Vladlen Koltun. Free view synthesis. In *Computer Vision–ECCV 2020: 16th European Conference, Glasgow, UK, August 23–28, 2020, Proceedings, Part XIX 16*, pages 623–640. Springer, 2020.
- [50] Gernot Riegler and Vladlen Koltun. Stable view synthesis. In *Proceedings of the IEEE/CVF Conference on Computer Vision and Pattern Recognition*, pages 12216–12225, 2021.
- [51] Barbara Roessle, Jonathan T Barron, Ben Mildenhall, Pratul P Srinivasan, and Matthias Nießner. Dense depth priors for neural radiance fields from sparse input views. In *Proceedings of the IEEE/CVF Conference on Computer Vision and Pattern Recognition*, pages 12892–12901, 2022.
- [52] Daniel Scharstein and Richard Szeliski. A taxonomy and evaluation of dense two-frame stereo correspondence algorithms. *International journal of computer vision*, 47:7–42, 2002.

- [53] Daniel Scharstein, Heiko Hirschmüller, York Kitajima, Greg Krathwohl, Nera Nesić, Xi Wang, and Porter Westling. High-resolution stereo datasets with subpixel-accurate ground truth. In Xiaoyi Jiang, Joachim Hornegger, and Reinhard Koch, editors, *GCPR*, volume 8753 of *Lecture Notes in Computer Science*, pages 31–42. Springer, 2014. ISBN 978-3-319-11751-5.
- [54] Johannes Lutz Schönberger and Jan-Michael Frahm. Structure-from-motion revisited. In *Conference on Computer Vision and Pattern Recognition (CVPR)*, 2016.
- [55] Johannes Lutz Schönberger, Enliang Zheng, Marc Pollefeys, and Jan-Michael Frahm. Pixelwise view selection for unstructured multi-view stereo. In *European Conference on Computer Vision (ECCV)*, 2016.
- [56] Thomas Schops, Johannes L Schönberger, Silvano Galliani, Torsten Sattler, Konrad Schindler, Marc Pollefeys, and Andreas Geiger. A multi-view stereo benchmark with high-resolution images and multi-camera videos. In *Proceedings of the IEEE conference on computer vision and pattern recognition*, pages 3260–3269, 2017.
- [57] Steven M Seitz, Brian Curless, James Diebel, Daniel Scharstein, and Richard Szeliski. A comparison and evaluation of multi-view stereo reconstruction algorithms. In *2006 IEEE computer society conference on computer vision and pattern recognition (CVPR'06)*, volume 1, pages 519–528. IEEE, 2006.
- [58] Elisavet Konstantina Stathopoulou and Fabio Remondino. A survey on conventional and learning-based methods for multi-view stereo. *The Photogrammetric Record*, 38 (183):374–407, 2023.
- [59] Cheng Sun, Min Sun, and Hwann-Tzong Chen. Direct voxel grid optimization: Superfast convergence for radiance fields reconstruction. In *Proceedings of the IEEE/CVF Conference on Computer Vision and Pattern Recognition*, pages 5459–5469, 2022.
- [60] Fabio Tosi, Alessio Tonioni, Daniele De Gregorio, and Matteo Poggi. Nerf-supervised deep stereo. In *Conference on Computer Vision and Pattern Recognition (CVPR)*, pages 855–866, June 2023.
- [61] Fabio Tosi, Luca Bartolomei, and Matteo Poggi. A survey on deep stereo matching in the twenties. *arXiv preprint arXiv:2407.07816*, 2024.
- [62] Dor Verbin, Peter Hedman, Ben Mildenhall, Todd Zickler, Jonathan T Barron, and Pratul P Srinivasan. Ref-nerf: Structured view-dependent appearance for neural radiance fields. In *2022 IEEE/CVF Conference on Computer Vision and Pattern Recognition (CVPR)*, pages 5481–5490. IEEE, 2022.
- [63] Chen Wang, Jiadai Sun, Lina Liu, Chenming Wu, Zhelun Shen, Dayan Wu, Yuchao Dai, and Liangjun Zhang. Digging into depth priors for outdoor neural radiance fields. *Proceedings of the 31th ACM International Conference on Multimedia*, 2023.
- [64] Guangcong Wang, Zhaoxi Chen, Chen Change Loy, and Ziwei Liu. Sparsenerf: Distilling depth ranking for few-shot novel view synthesis. *arXiv preprint arXiv:2303.16196*, 2023.

- [65] Xiang Wang, Chen Wang, Bing Liu, Xiaoqing Zhou, Liang Zhang, Jin Zheng, and Xiao Bai. Multi-view stereo in the deep learning era: A comprehensive review. *Displays*, 70:102102, 2021.
- [66] Yi Wei, Shaohui Liu, Yongming Rao, Wang Zhao, Jiwen Lu, and Jie Zhou. Nerfingmvs: Guided optimization of neural radiance fields for indoor multi-view stereo. In *Proceedings of the IEEE/CVF International Conference on Computer Vision*, pages 5610–5619, 2021.
- [67] Zexiao Xie, Xiaoxuan Yu, Xiang Gao, Kunqian Li, and Shuhan Shen. Recent advances in conventional and deep learning-based depth completion: A survey. *IEEE Transactions on Neural Networks and Learning Systems*, 2022.
- [68] Dejia Xu, Yifan Jiang, Peihao Wang, Zhiwen Fan, Humphrey Shi, and Zhangyang Wang. Sinnerf: Training neural radiance fields on complex scenes from a single image. In *European Conference on Computer Vision*, pages 736–753. Springer, 2022.
- [69] Qiangeng Xu, Zexiang Xu, Julien Philip, Sai Bi, Zhixin Shu, Kalyan Sunkavalli, and Ulrich Neumann. Point-nerf: Point-based neural radiance fields. In *Proceedings of the IEEE/CVF Conference on Computer Vision and Pattern Recognition*, pages 5438–5448, 2022.
- [70] Xiaoqiang Yan, Shizhe Hu, Yiqiao Mao, Yangdong Ye, and Hui Yu. Deep multi-view learning methods: A review. *Neurocomputing*, 448:106–129, 2021.
- [71] Yao Yao, Zixin Luo, Shiwei Li, Tian Fang, and Long Quan. Mvsnet: Depth inference for unstructured multi-view stereo. In *Proceedings of the European Conference on Computer Vision (ECCV)*, pages 767–783, 2018.
- [72] Yao Yao, Zixin Luo, Shiwei Li, Jingyang Zhang, Yufan Ren, Lei Zhou, Tian Fang, and Long Quan. Blendedmvs: A large-scale dataset for generalized multi-view stereo networks. In *Proceedings of the IEEE/CVF Conference on Computer Vision and Pattern Recognition*, pages 1790–1799, 2020.
- [73] Chandan Yeshwanth, Yueh-Cheng Liu, Matthias Nießner, and Angela Dai. Scannet++: A high-fidelity dataset of 3d indoor scenes. In *Proceedings of the International Conference on Computer Vision (ICCV)*, 2023.
- [74] Wang Yifan, Felice Serena, Shihao Wu, Cengiz Öztireli, and Olga Sorkine-Hornung. Differentiable surface splatting for point-based geometry processing. *ACM Transactions on Graphics (TOG)*, 38(6):1–14, 2019.
- [75] Alex Yu, Ruilong Li, Matthew Tancik, Hao Li, Ren Ng, and Angjoo Kanazawa. Plenotrees for real-time rendering of neural radiance fields. In *Proceedings of the IEEE/CVF International Conference on Computer Vision*, pages 5752–5761, 2021.
- [76] Zehao Yu, Songyou Peng, Michael Niemeyer, Torsten Sattler, and Andreas Geiger. Monosdf: Exploring monocular geometric cues for neural implicit surface reconstruction. *Advances in neural information processing systems*, 35:25018–25032, 2022.
- [77] Jiayi Zeng, Chengtang Yao, Lidong Yu, Yuwei Wu, and Yunde Jia. Parameterized cost volume for stereo matching. In *Proceedings of the IEEE/CVF International Conference on Computer Vision*, pages 18347–18357, 2023.

-
- [78] Kai Zhang, Gernot Riegler, Noah Snaveley, and Vladlen Koltun. Nerf++: Analyzing and improving neural radiance fields. *arXiv preprint arXiv:2010.07492*, 2020.
- [79] Qiang Zhang, Seung-Hwan Baek, Szymon Rusinkiewicz, and Felix Heide. Differentiable point-based radiance fields for efficient view synthesis. In *SIGGRAPH Asia 2022 Conference Papers*, pages 1–12, 2022.
- [80] Chaoqiang Zhao, Qiyu Sun, Chongzhen Zhang, Yang Tang, and Feng Qian. Monocular depth estimation based on deep learning: An overview. *Science China Technological Sciences*, 63(9):1612–1627, 2020.
- [81] Kun Zhou, Xiangxi Meng, Bo Cheng, et al. Review of stereo matching algorithms based on deep learning. *Computational intelligence and neuroscience*, 2020, 2020.